J. Fluid Mech. (1983), *vol.* 127, *pp.* 1–25
Printed in Great Britain

Pulsatile entrance flow in a curved pipe

By L. TALBOT AND K. O. GONG†
Department of Mechanical Engineering, University of California, Berkeley

(Received 30 April 1982)

An experimental investigation was made of the entry flow in a curved pipe under conditions wherein a pulsatile component of flow was superimposed on a steady mean flow. Two experiments were conducted, one in a pipe of curvature ratio $\delta = \frac{1}{20}$ under conditions of Womersley parameter $\alpha_w = 8{\cdot}0$ and alternative Dean number $\kappa = 120$, the second in a pipe of $\delta = \frac{1}{7}$ for $\alpha_w = 12{\cdot}5$ and $\kappa = 372$. Laser-velocimetry measurements of the axial and secondary velocities were made throughout the cross-section at different instants of time within the cycle and at several axial locations downstream from the pipe entrance.

The flow in the first experiment was found to be quasisteady, with axial and secondary velocities varying in time at the several axial stations proportionally to the instantaneous mean velocity, but essentially the same in character as low-Dean-number steady entry flow. The flow in the second experiment was more complex, with separation of the axial flow appearing at the inner bend during deceleration, starting downstream and propagating upstream toward the pipe entrance. Helical motions imbedded within the Dean circulation were also observed, and during certain portions of the cycle the secondary motions within the central core took on a jet-like structure.

It suggested that the classifications employed by Smith to describe the different regimes of fully-developed pulsatile flow in curved pipes may also be useful to distinguish between different entry-flow regimes.

1. Introduction

The nature of flow development in the entry region of a curved circular pipe is not only of interest as a fundamental fluid-mechanical problem but also because of its relevance to engineering and haemodynamic problems. The most recent interest in curved-pipe entry flow has been largely stimulated by the suspicion that fluid mechanics may play a role in atherogenesis. The possible connections between fluid mechanics and arterial disease have been discussed by many authors (e.g. Nerem & Cornhill 1980) and need not be repeated in detail here. It is sufficient to note that the patterns of aortic lesions found in the aortic arch have prompted some researchers to conjecture that regions of large curvature and large excursions in wall shear-stress levels may be among the favoured sites for atherogenesis.

The complex flow patterns that occur in the entry region of a curved vessel are such that, in order to identify a fluid-dynamical phenomenon as a possible contributory factor to the development of lesions, detailed knowledge of the flow must first be gained, and it is to this end that the present study is directed. We treat here the problem of pulsatile entry flow in a curved pipe purely as an experimental fluid-dynamical one, leaving aside questions pertaining to the role the fluid motions might play in the initiation of atherosclerosis.

In an earlier study by Agrawal, Talbot & Gong (1978) laser-velocimetry measure-

† Present address: IBM Corp., Tucson, Arizona, U.S.A.

ments were made of the axial and secondary velocities in the entry region of curved pipes under steady flow conditions. This study, hereinafter referred to as I, exposed a number of interesting features of the flow, including the formation of imbedded helical motions within the Dean circulation, and three-dimensional separation at the inner wall due to collision of the secondary motion boundary layers. This study was followed by an investigation by Choi, Talbot & Cornet (1979) of the wall shear distribution, using an electrochemical measurement technique, which identified certain correlations between velocity patterns and wall shear variations. The present study extends the work of I to the case of pulsatile flow, which of course is of more physiological interest.

2. Experimental apparatus

The flow system employed in the present experiments, shown in figure 1, is the same as that described in I, with the exception of the addition of a flow control valve, which was used to create the pulsatile component of the flow. This valve was a $1\frac{1}{2}$ in. gate valve driven by a 200 step/revolution stepping motor, and controlled by a PDP-8L minicomputer. By programmed selection of the time intervals between computer pulses to the stepping motor, essentially any desired flow-rate waveform could be produced. The flow system, having a constant-head tank supply, was restricted to positive flow conditions, although, when the valve was closed rapidly, a very small amount of backflow resulted because of the compliance of the system.

The laser-velocimeter system used was similar to that employed in the earlier study, except that a rotating holographic grating bleached for maximum intensity in first order was used as the beam splitter and frequency-shifting device for both of the velocity components measured. The photomultiplier output was filtered and amplified with a TSI 1057 Signal Conditioner and then sampled by a TSI 1090 Signal Processor, which gives an analog voltage output linearly related to the Doppler frequency. The sampled output voltages were digitized by an A/D converter, and stored in the memory of the PDP-8L computer for subsequent transfer to a Kennedy Digital

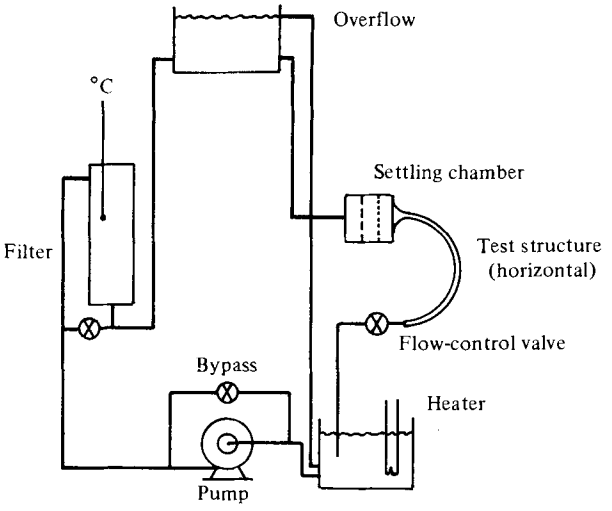

FIGURE 1. Schematic diagram of the flow facility.

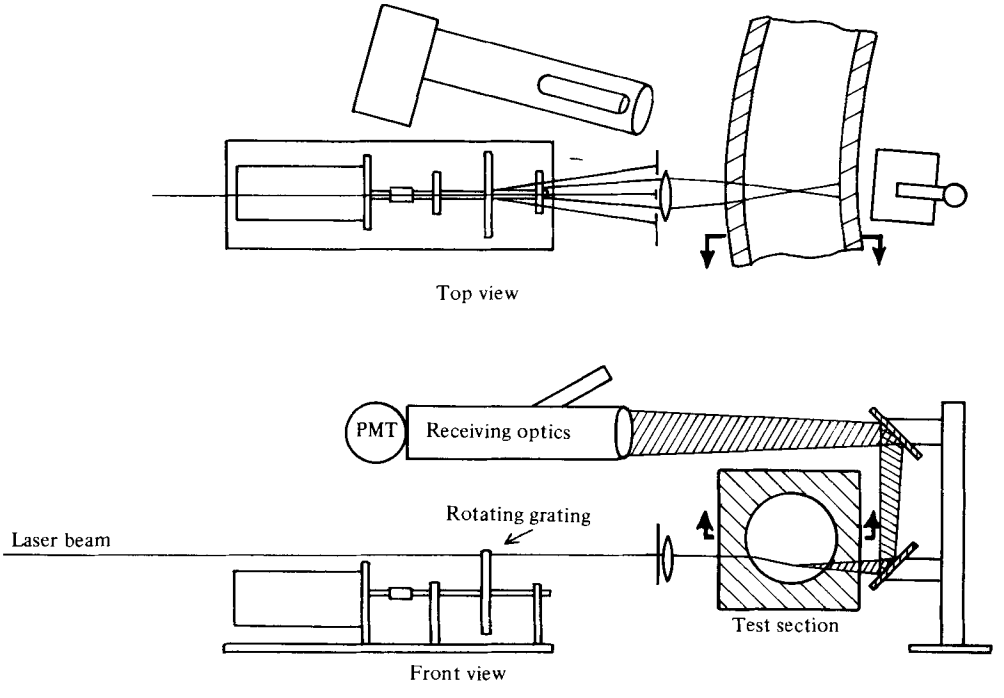

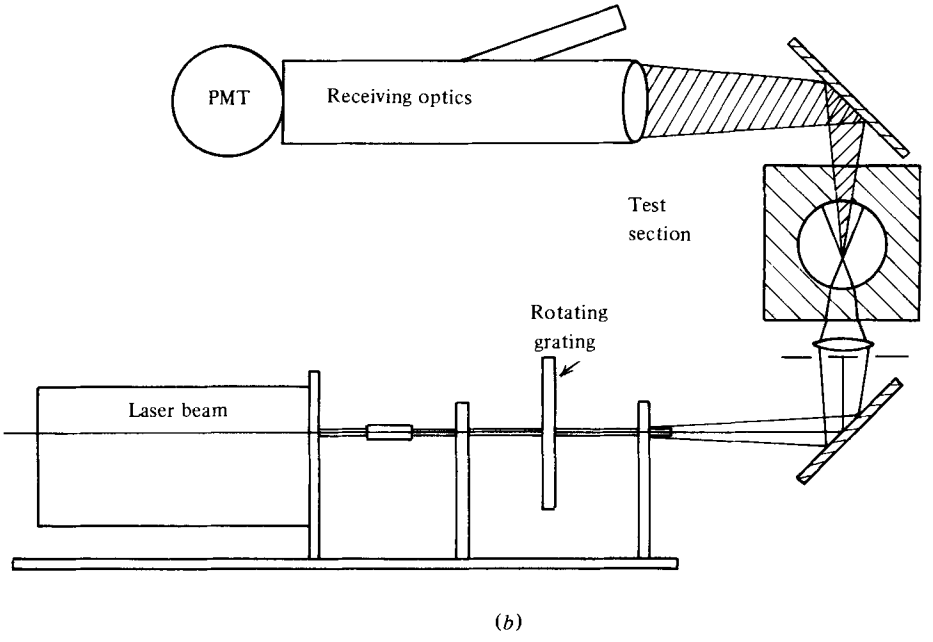

FIGURE 2. (*a*) Optical configuration for W-velocity measurement. (*b*) Optical configuration for U-velocity measurement.

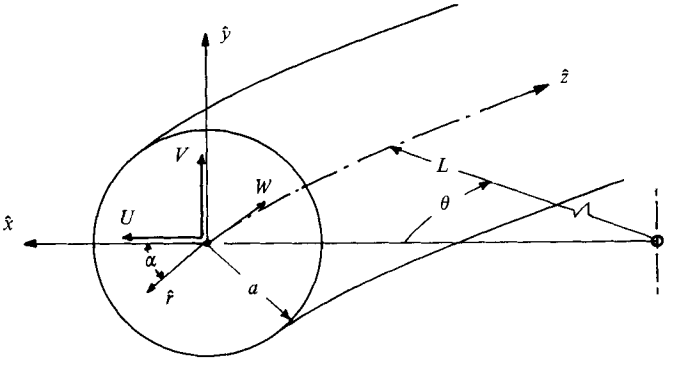

FIGURE 3. Coordinate system and velocity notation.

Magnetic Tape recorder. The magnetic tape format was compatible with that of the Berkeley Campus CDC 6400 computer, thus making it possible for data analysis and plotting to be carried out at the Computer Center. The arrangements of the optics for the two velocity component measurements are shown in figures 2(*a*, *b*).

As in I, the circulating fluid was a mixture of glycerol and water, which provided a reasonably close index of refraction matching with the lucite test sections, and also provided a convenient means of varying the flow Reynolds number simply by changing the proportions of glycerol and water in the mixture. In the first experiment to be described, the percentage of glycerol was about 63%. This percentage was reduced by a factor of about 3 for the second experiment. The corresponding kinematic viscosities were $\nu = 1{\cdot}2 \times 10^{-1}$ cm^2/s for experiment 1 and $\nu = 3{\cdot}5 \times 10^{-2}$ cm^2/s for experiment 2. Dow Chemical plastic paint pigment 722 was used as the seeding material for the laser-velocimetry measurements.

The two 180° curved-pipe test sections used in I were also employed in the present studies. The internal radius a of both test sections was 1·905 cm. The radii of curvature L of the sections were such that for one pipe $\delta = a/L = \frac{1}{20}$, while for the other $\delta = \frac{1}{7}$. The coordinate system and the velocity notation used in describing the velocity measurements ares shown in figure 3. The outer generator of the bend is at $\alpha = 0$, $x = \hat{x}/a = 1$, and the inner generator of the bend is at $\alpha = \pi$, $x = -1$. ('Hat' variables are dimensional.)

3. Experimental procedures

Measurements were first carried out on the pipe with curvature ratio $\delta = \frac{1}{20}$. For this pipe the stepping-motor programme was adjusted by repeated trial until a sinusoidal flow-rate waveform was obtained, which as shown in figure 4(*a*) was of the form

$$Q = Q_{\mathrm{DC}} + Q_{\mathrm{AC}} \cos(\omega t - \phi) \tag{1}$$

with $Q_{\mathrm{DC}} = 0{\cdot}1922$ litres/s, $Q_{\mathrm{AC}} = 0{\cdot}0647$ litres/s, $\omega = 2{\cdot}11$ rad/s and $\phi = 0{\cdot}0563$. The non-dimensional parameters associated with this flow were $\alpha_{\mathrm{w}} = a(\omega/\nu)^{\frac{1}{2}} = 8{\cdot}0$ and $\kappa = 2W_0 a\delta^{\frac{1}{2}}/\nu = 110$, where ν is the kinematic viscosity and W_0 is the mean axial velocity. α_{w} and κ are sometimes referred to as the Womersley parameter and the mean alternative Dean number respectively.

Axial velocities were measured at 62 points in the cross-section, located at rectangular grid points below the centreplane ($\alpha = 0, \pi$), this arrangement having

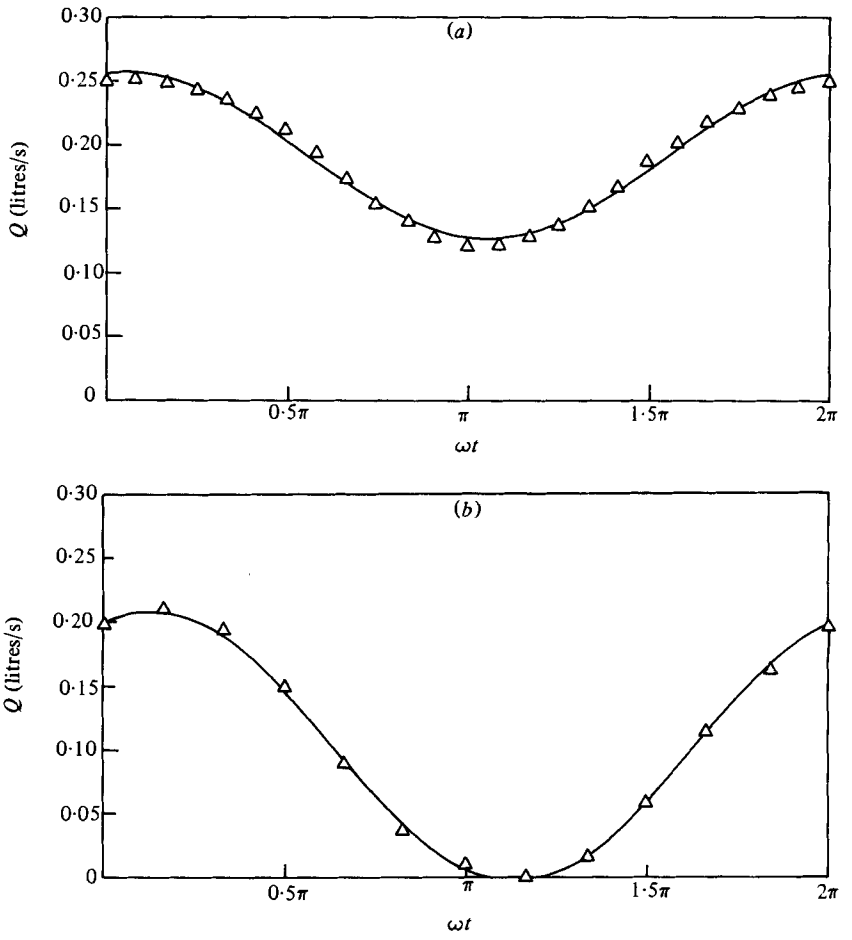

FIGURE 4. Experimental flow conditions: (*a*) experiment 1; (*b*) experiment 2. △, data; ——, least-squares fit.

been selected to take advantage of available numerical methods and surface display plotting routines. Approximately 150 grid points were used for the U-component measurements. Only the lower half of the cross-section was investigated, since an independent set of measurements verified that, within experimental uncertainty, there was flow symmetry about the centreplane.

At each grid point, velocity data were taken at $\frac{1}{12}\pi$ cycle intervals, giving 24 velocity–time data for a cycle. This was repeated for eight consecutive cycles. The data were stored in computer memory as they were taken, and displayed on an oscilloscope, superimposing the eight cycles upon one another. If cycle-to-cycle variations were judged not to be present the eight cycles of data were averaged into one cycle and stored. When the limited memory of the PDP-8L computer was filled, the data were transferred to the magnetic tape, and the process repeated. During the few seconds required for the data transfer, the minicomputer control of the control valve was interrupted, and the flow cycle halted. Cyclic variations initially were present upon resumption of the flow, but after about four or five cycles they disappeared and the data-acquisition process was resumed until the next data transfer was required.

In experiment 2 on the $\delta = \frac{1}{7}$ test section, the flow parameters were chosen so as to correspond more nearly to those of the human aortic arch. The least-squares fit to (1) shown in figure 4(*b*) yielded the values $Q_{DC} = 0{\cdot}1031$ litres/s, $Q_{AC} = 0{\cdot}1055$ litres/s, $\phi = 0{\cdot}134$ and $\omega = 1{\cdot}51$ rad/s: These correspond to parameter values $\alpha_w = 12{\cdot}5$ and $\kappa = 372$. Axial- and secondary-velocity data were obtained at streamwise stations $\hat{z}/L = \theta = 15°$, 30°, 60° and 110°. The cycle was divided up into $\frac{1}{6}\pi$ intervals, so that there were 12 velocity–time data per cycle at each point of measurement. The data-acquisition procedures were the same as those used in experiment 1.

4. Limitations and uncertainties of the experiments

The cemented interfaces at the $\alpha = (0, \pi)$ planes of symmetry of the two test sections caused several problems. Not only did they preclude the measurement of the V-component of velocity, they also prevented the measurement of the W-component at the midplane, and data could not be obtained for $|\hat{y}/a| = |y| \lesssim 0{\cdot}066$. Imperfect matching of the indices of refraction of the lucite and the glycerol–water solutions also caused problems. In addition to requiring that Snell's law be employed in the data-acquisition procedure to position each grid point at which velocities were measured, the refractive-index mismatch resulted in the inclusion of a portion of the V-component of velocity in the U-component of velocity being measured. This effect was most severe in the U-component measurements in the neighbourhood of $y = 0$, $x = \pm 1$, the inner and outer walls of the bends. The probable error in the U-component measurement due to this effect is estimated to be approximately

$$(1 - \cos\gamma + \sin\gamma)/(1 - \sin\gamma),$$

where $\gamma = \tan^{-1}(V/U)$. For experiment 1, using refractive-index values $\mu_\ell = 1{\cdot}4895$ for lucite and $\mu_m = 1{\cdot}419$ for the mixture, the estimate of γ was typically 1–2°, with a maximum of 6°. In experiment 2, with $\mu_m = 1{\cdot}3785$, γ was estimated to be typically 1–3°, with a maximum of about 10°. The mixture refractive indices were obtained with a Pulfrich refractometer, which had an uncertainty of $\pm 0{\cdot}005$.

The probable errors in the axial velocities, due to phase noise from multiple particle scattering, grating-frequency fluctuations and the one-bit uncertainty in the A/D signal conversion, were about 0·05 cm/s absolute and less than 5 % relative. The uncertainty in the secondary-velocity measurement was due mainly to the refractive effects described. For $\gamma = 3°$, it was about 6 %, whereas for the maximum value $\gamma = 10°$, it was about 20 %.

The positional accuracy with which the measured data corresponded to their assigned rectangular grid points was within 0·05 mm except for two points in experiment 1 which were later corrected. The uncertainly in the viscosity, as measured by a Saybolt viscosimeter, was about 10 %, and the uncertainty in the flow-rate values Q_{AC} and Q_{DC}, as obtained by integration of the axial-velocity profiles, was about 3 %. These combine to give an uncertainty of about 10 % in κ and about 4 % in α_w. The uncertainty in ω was negligible.

5. Experimental results

5.1. *The first experiment*

The conditions for experiment 1 in the $\delta = \frac{1}{20}$ pipe were $Q_{AC}/Q_{DC} \approx 0{\cdot}34$, $\alpha_w = 8{\cdot}0$ and $\kappa = 120$. Of the 24 time intervals within the cycle at which data were obtained, only 6 are presented here. Also, although measurements were made at streamwise

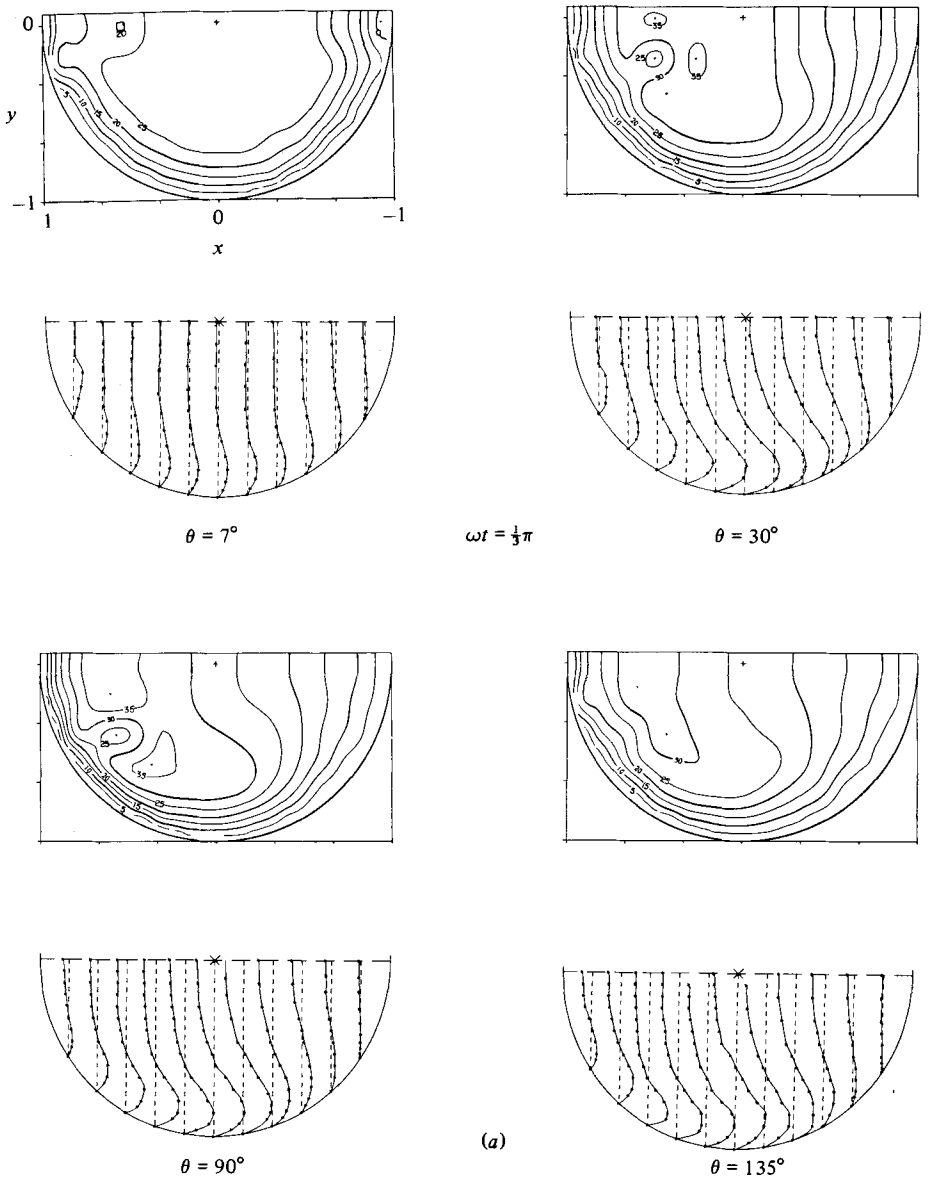

FIGURE 5(*a*). For caption see p. 12.

locations $\theta = 7°$, 30°, 60°, 90° and 135°, we have omitted the 60° data since it was quite similar to the 90° data. Some of the omitted data are reported in Gong (1979).

The data for experiment 1 are given in figures 5(*a–f*), corresponding to the instants of time $\omega t = \frac{1}{3}n\pi$ (n = 1–6) within the cycle. Each figure contains four data sets, corresponding to the four θ-locations. In each data set, the upper panel displays the W-isovelocity contours (isotachs) labelled in values of cm/s and the lower panel the U-velocity profiles. Crosses within isotach contours indicate local maxima or minima. The zeros of the U-profiles are indicated by the vertical broken lines, and the scale for U is such that the spacing between these lines corresponds to 4 cm/s. The phase angle for these data was $\phi = 0{\cdot}056\pi$. Thus the first time instant exhibited in figure

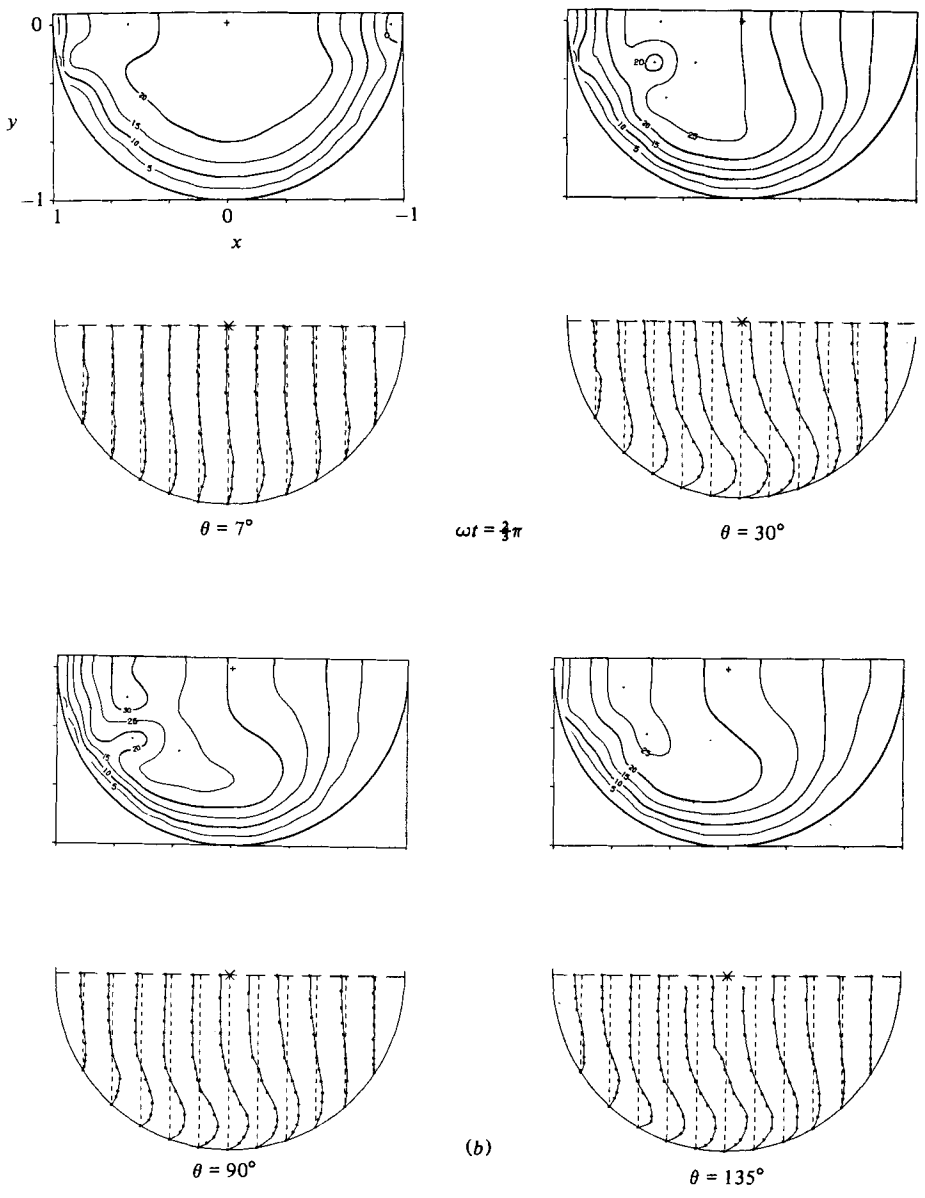

FIGURE 5(*b*). For caption see p. 12.

5 (*a*), $\omega t = \frac{1}{3}\pi$, occurred slightly after the onset of deceleration following peak flow rate.

Several interesting features are evident in the data exhibited in figure 5(*a*). At the first axial station, $\theta = 7°$, we observe essentially concentric isotachs over most of the cross-section, indicative of a nearly symmetric axial-velocity entry profile. However, in the vicinities of $x = \pm 1$ and $y = 0$, there are inward displacements of the isotachs, indicating retardation and probably separation of the flow in these regions. (The outward bulge in the 20 cm/s isotach at $x \approx 0{\cdot}9$, $y \approx -0{\cdot}25$ is an artefact – this was the place where a grid point was incorrectly located.) The character of the flow in these regions will be discussed in more detail later on.

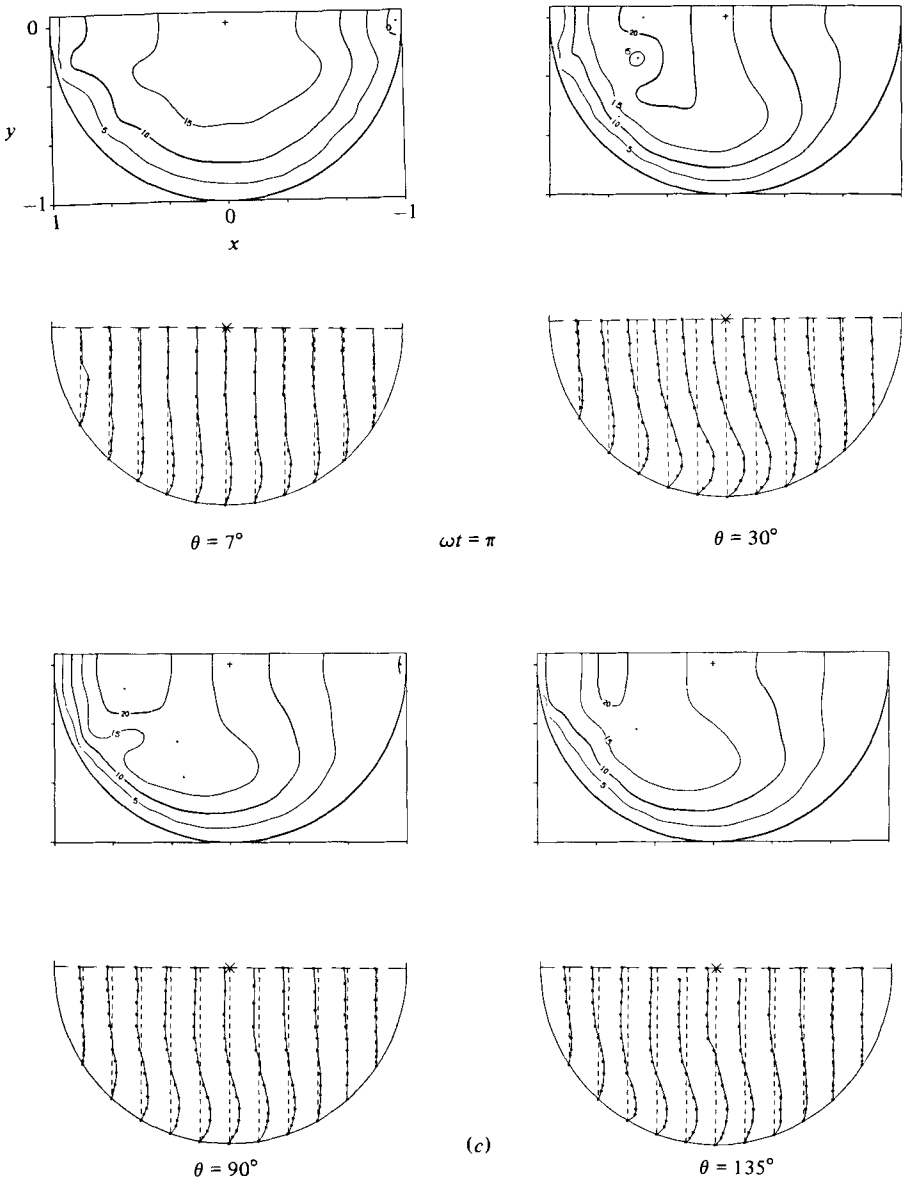

FIGURE 5(*c*). For caption see p. 12.

Farther downstream, at $\theta = 30°$ it is seen that the region of retarded core flow which appeared at the outer bend at $\theta = 7°$ has been convected downward, presumably by the secondary Dean circulation. Since the flow is symmetrical about $y = 0$, the same process has occurred in the upper half of the cross-section. The downward motion of this region continues at $\theta = 90°$. However, at the farthermost-downstream axial station, $\theta = 135°$, the region has disappeared, and the isotachs are representative of the fully developed velocity profile measured by Adler (1934), as seen in figure 6.

The secondary U-velocity profiles at the four θ-stations shown in figure 5(*a*) all exhibit the same Dean circulation pattern. The circulation strength is smallest at the

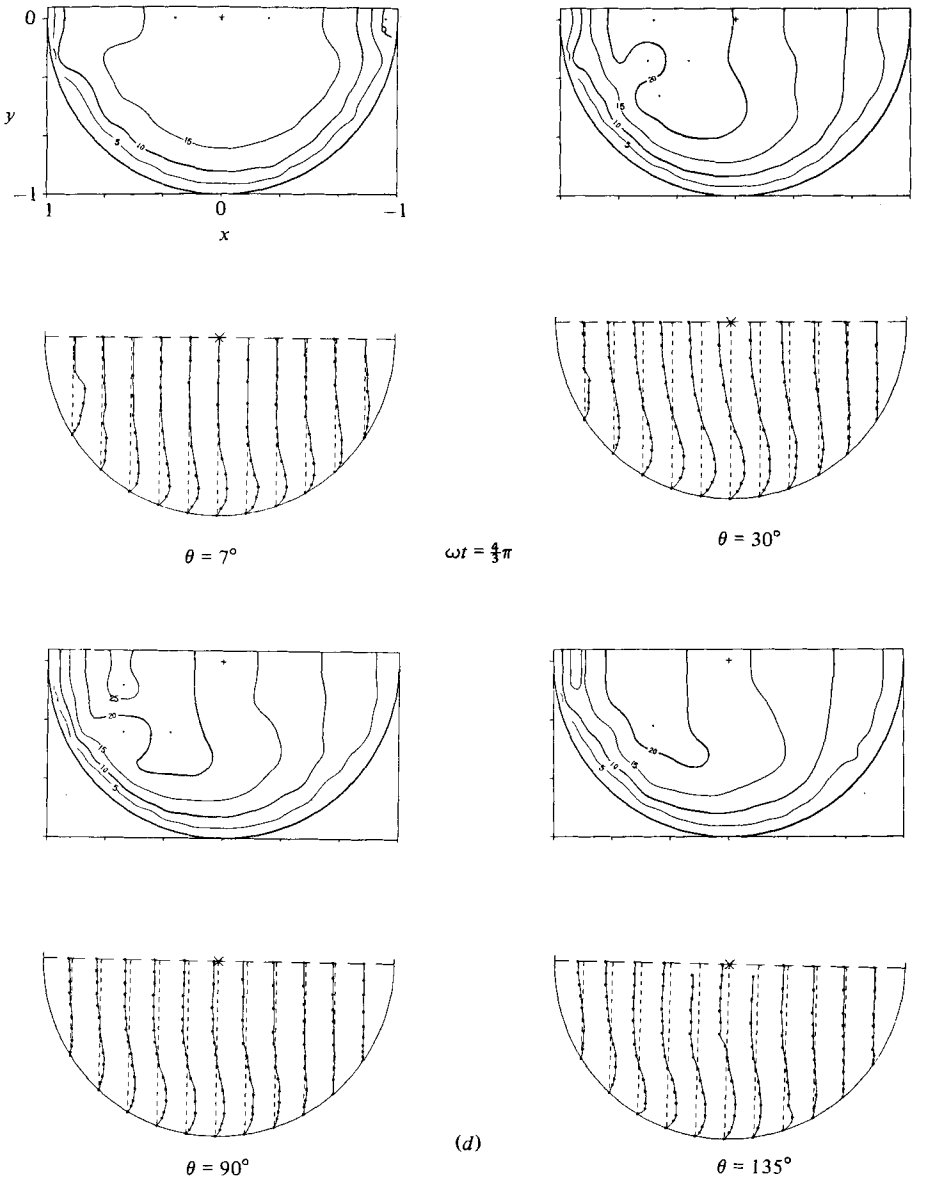

FIGURE 5(*d*). For caption see p. 12.

first axial station, reaches a maximum in the vicinity of $\theta = 30°$, and levels off to essentially a constant value downstream at $\theta = 90°$ and 135°.

The flow patterns that evolve as a function of time throughout the cycle are shown in the remaining frames of figure 5. Both the isotachs and the U-velocity profiles at corresponding axial locations are remarkably similar for the six values of ωt, the only essential differences being in the numerical magnitudes of the velocities. In other words, the conditions of this experiment were such that the flow could be described as essentially quasisteady.

As mentioned above, flow separation probably was present in the vicinities of $x = \pm 1$ at the first streamwise station, $\theta = 7°$. The inward displacement of the

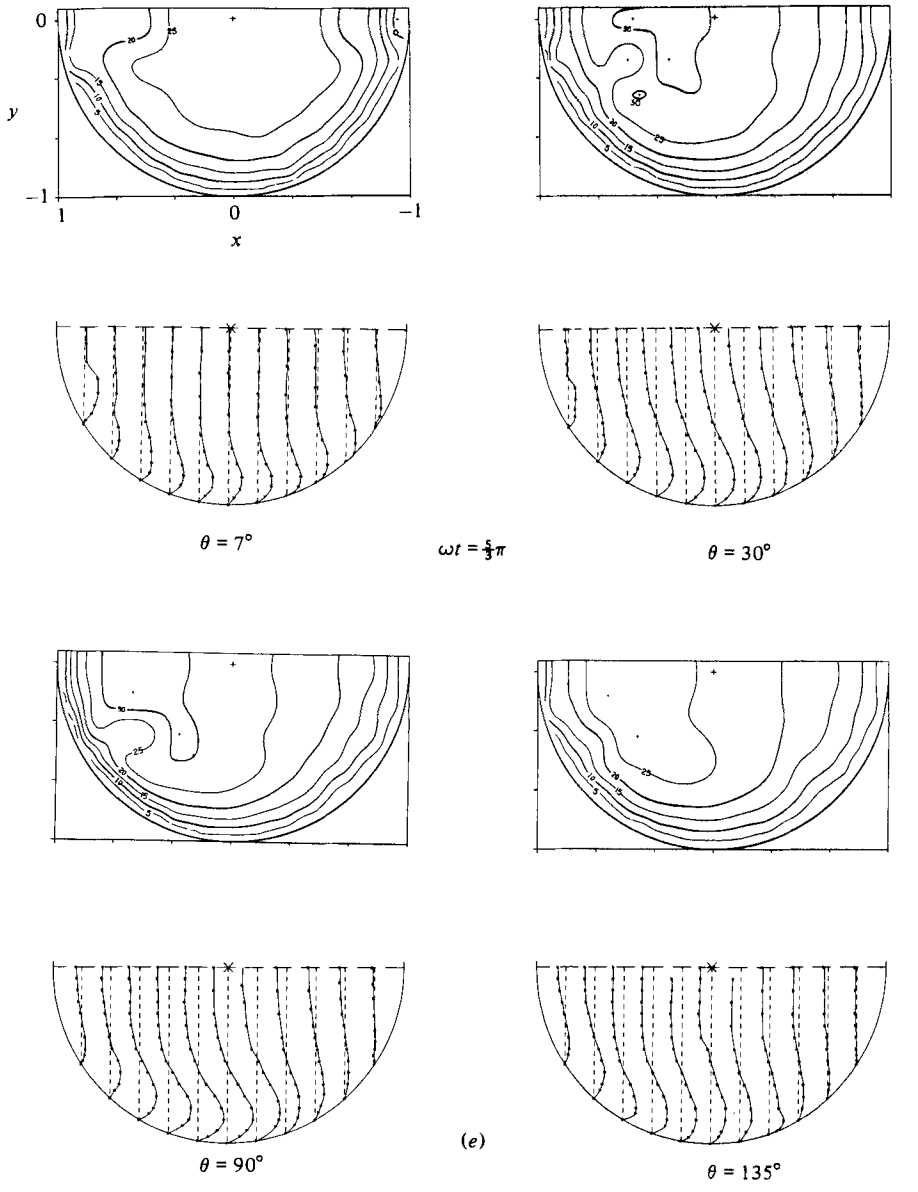

FIGURE 5(*e*). For caption see p. 12.

isotachs at the outer wall ($x \approx 1$) strongly suggests that the separation line is of a local type, in the terminology of Tobak & Peake (1982), wherein the skin-friction line on which other lines converge does not originate from a saddle point. This may also be the case for the separation at the inner wall as well, although it is possible that it is a global-type separation, with a structure similar to that found ahead of a small protuberance within a boundary layer.

The separated regions probably have their origins at the junction between the trumpet-shaped inlet and the curved pipe. At the outer wall, the boundary layer experiences a sudden rise in pressure of order $\rho W_0^2 \delta$ due to pipe curvature, while, at the inner wall, wall convexity may be contributory to separation. Interestingly,

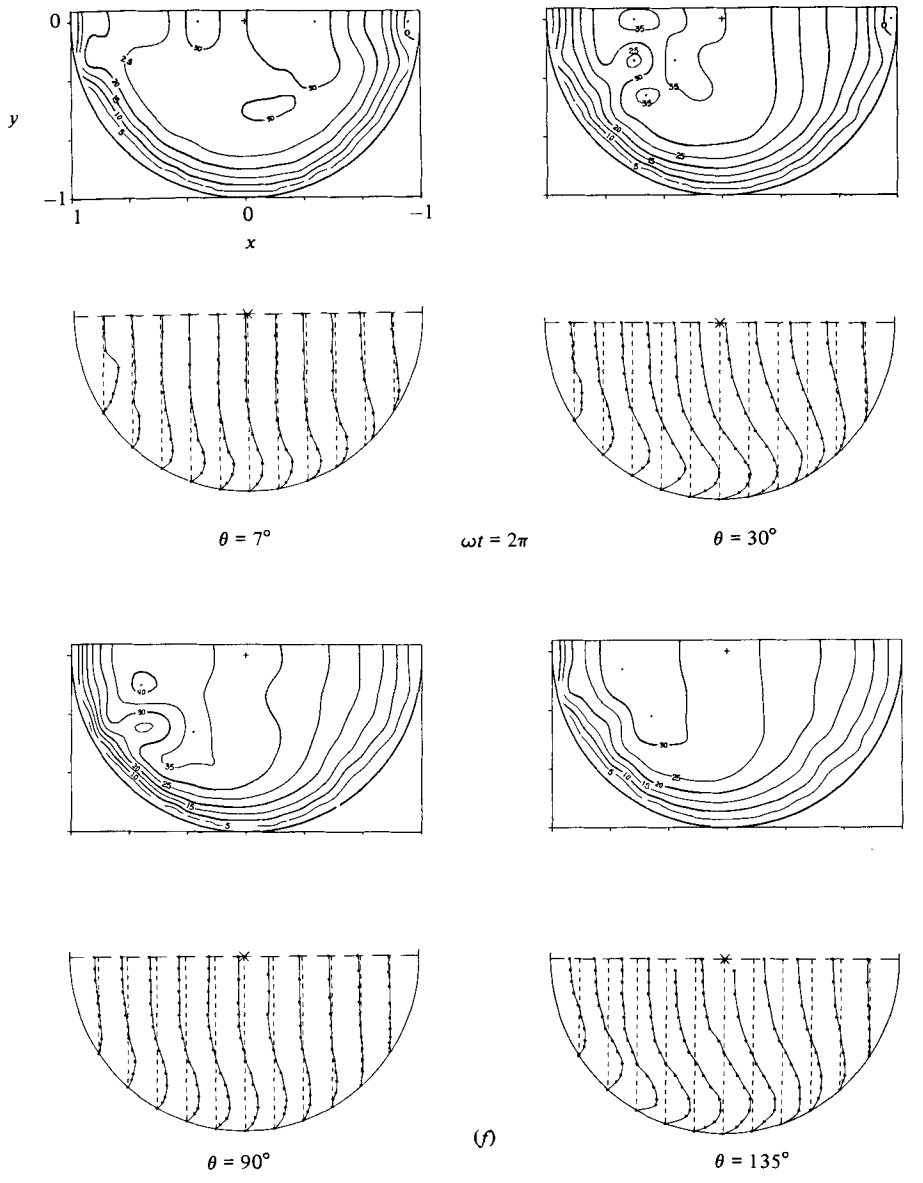

FIGURE 5. W-velocity isotachs and U-velocity profiles at different θ-locations at various instants of time in the cycle for experiment 1. (*a*)–(*f*): $\omega t = \frac{1}{3}n\pi$, $n = 1$–6.

however, separated flow was not observed in the steady-flow experiments of I in the same apparatus. One might conjecture that the unfavourable pressure gradients present during the decelerative phase of the flow together with curvature and wall-convexity effects combine to cause the separations, and that once created the separations persist thoughout the entire cycle, including the accelerative phase of the flow, because of flow hysteresis. If this is the correct explanation, it would be an example of a subcritical bifurcation as described by Tobak & Peake.

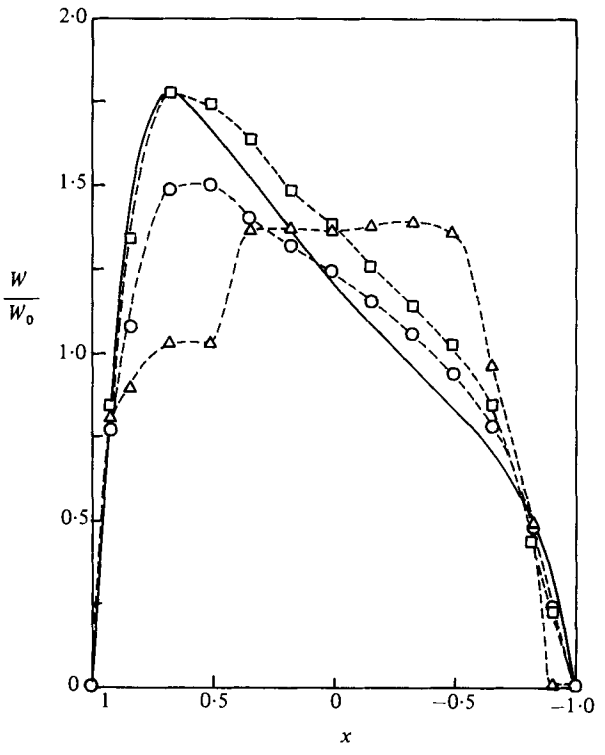

FIGURE 6. Centreplane axial-velocity profiles at different θ-locations for experiment 1 at $\omega t = 2\pi$: △, $\theta = 7°$; ○, 60°; □, 110°; ——, Adler (1934), $\kappa = 372$.

5.2. *The second experiment*

The conditions for experiment 2, as mentioned above, were $\delta = \frac{1}{7}$, $Q_{AC}/Q_{DC} = 1{\cdot}02$, $\omega = 1{\cdot}51$ rad/s, $\phi = 0{\cdot}134$, $\alpha_w = 12{\cdot}5$ and $\kappa = 372$. Data were obtained at streamwise stations $\theta = 15°$, 30°, 60° and 110°, and at instants of time $\omega t = \frac{1}{6}n\pi$ within the cycle ($n = 1$–12). We present here the data for $\omega t = \frac{1}{6}(2n+1)\,\pi$, $n = 0$–5; additional data are reported in Gong (1979).

The experiment 2 data are shown in figures 7(*a*–*f*). As for experiment 1, each figure contains four data sets, corresponding to the four streamwise θ-locations, for the particular time instant of the cycle. The upper panel of each data set displays the axial-velocity isotachs, labelled in cm/s, and the lower panel the U-velocity profiles. The scale for U is such that the spacing between vertical broken lines corresponds to 3 cm/s. Since the phase angle was $\phi = 0{\cdot}134\pi$, the data for the first time instant, $\omega t = \frac{1}{6}\pi$, corresponds to a time in the cycle following shortly after the onset of bulk flow deceleration.

Beginning with figure 7(*a*), at time $\omega t = \frac{1}{6}\pi$, we observe that at $\theta = 15°$ the axial flow resembles that of a potential vortex, except for the 20 cm/s contour for $x \gtrsim 0{\cdot}05$, since the highest axial velocities occur near the inner bend. This potential-like feature of the flow was present also in experiment 1, although less apparent, because of the smaller value of δ. The inward bulge of the 20 cm/s contour is similar to what was observed in experiment 1, and is most likely caused by flow separation as discussed earlier. Farther down the pipe, at successive streamwise stations $\theta = 30°$, 60° and 110°, one observes the shift of the axial velocity maximum toward the outer bend,

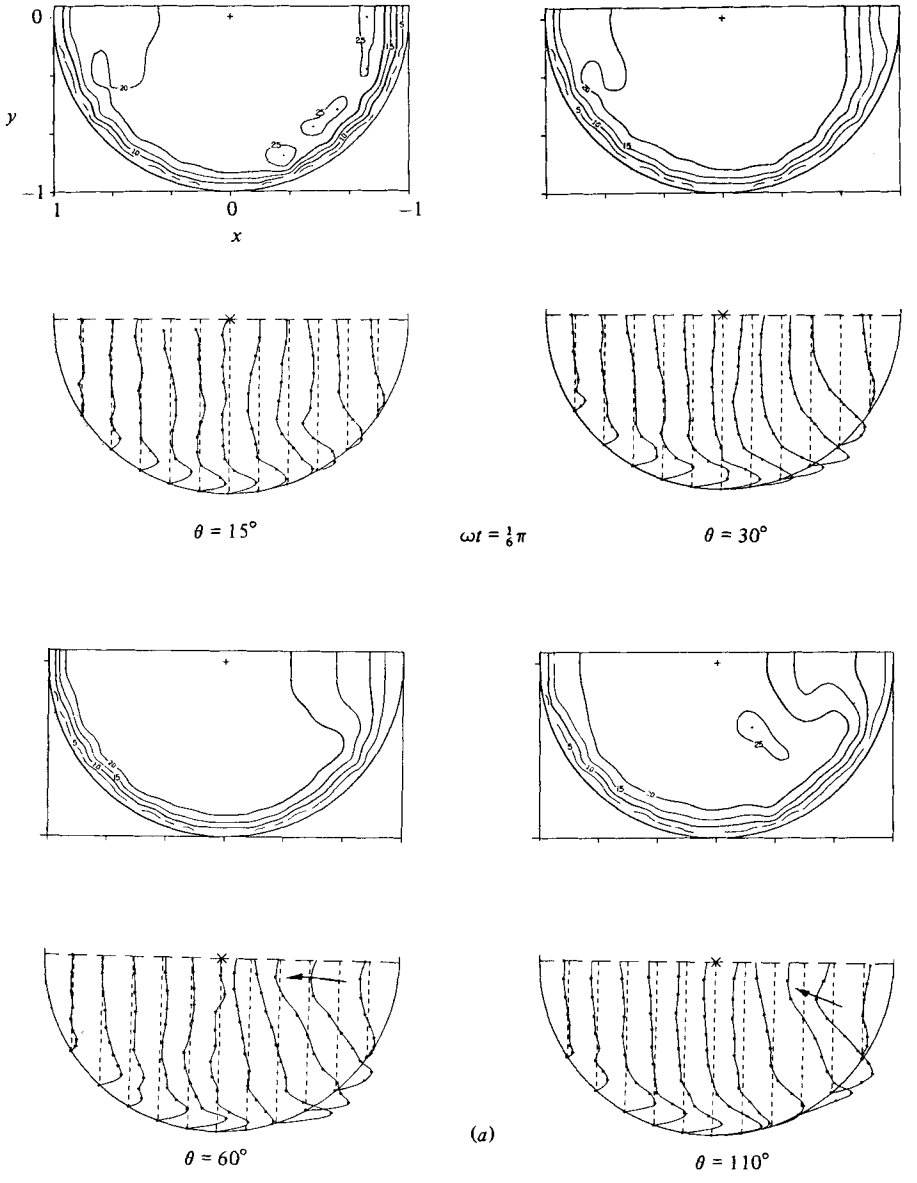

(a)

FIGURE 7 (a). For caption see p. 19.

and disappearance of inlet-flow distortion in the outer bend region. The most notable feature of the secondary flow at this instant in the cycle is the appearance of a jet-like outward motion at sections $\theta = 60°$ and 110°. This motion is associated with the growth of the axial boundary layer at the inner bend and the shift of the peak axial velocity toward the outer bend.

Figure 7 (*b*) displays the flow patterns at $\omega t = \frac{1}{2}\pi$, about a third of the way through the decelerative phase of the cycle. Reverse axial flow has occurred at the inside bend at the streamwise stations $\theta = 30°$, 60° and 110°, but has not yet propagated upstream to the $\theta = 15°$ location. The instantaneous axial-flow streamlines at this instant would be characteristic of a global-type separated region at the inner bend, with the saddle

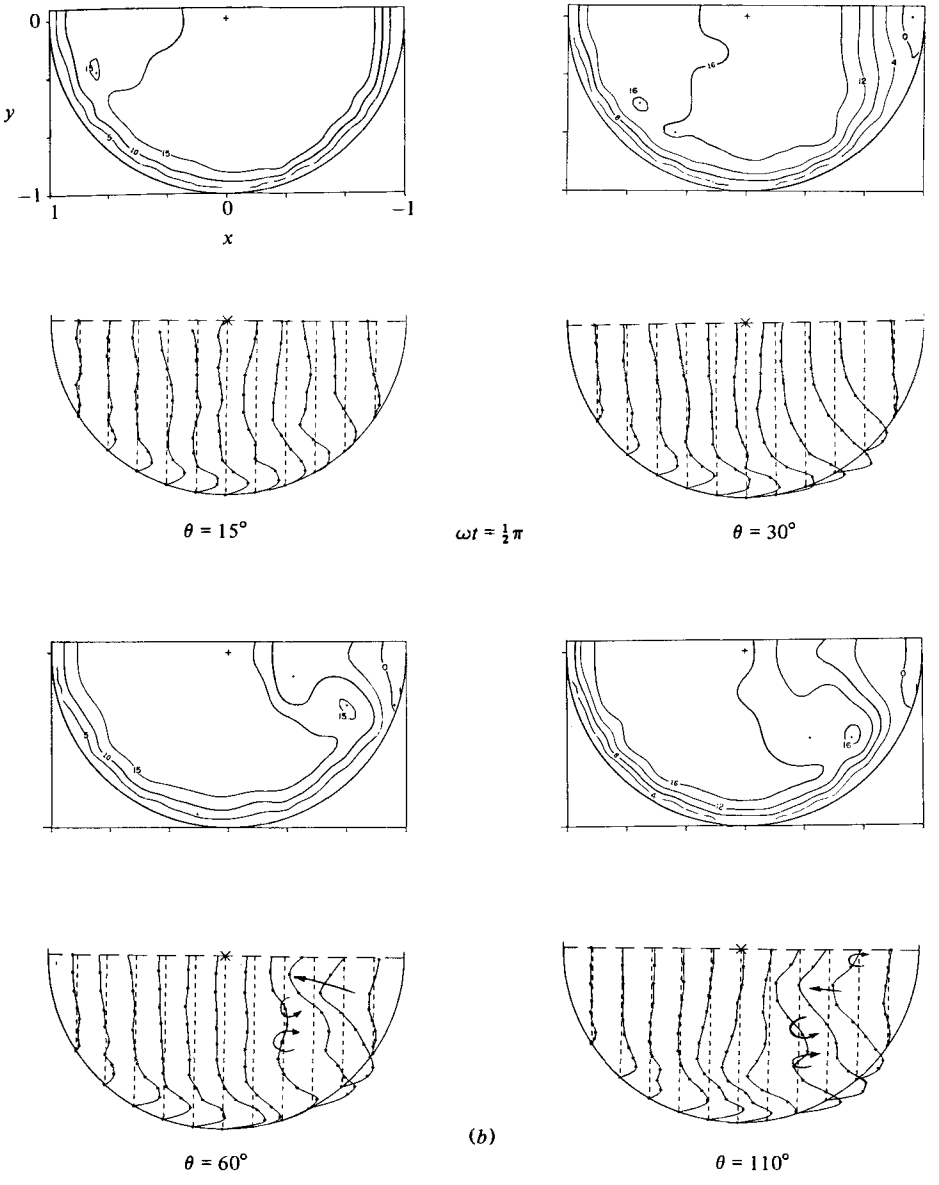

(*b*)

FIGURE 7 (*b*). For caption see p. 19.

point at the leading edge of the region located somewhere between $\theta = 15°$ and 30°. The isotachs at $\theta = 60°$ and 110° exhibit a local secondary maximum along a constant y-plane passing through the closed 15 and 16 cm/s contours, similar to the secondary maxima observed in I. Imbedded secondary-flow helical motions occur at the outer borders of the region occupied by the secondary maxima, as was also observed in I, their locations closely coinciding with the troughs of minimum velocity separating the two velocity maxima.

Figure 7 (*c*) exhibits the situation occurring at $\omega t = \frac{5}{6}\pi$, about two-thirds of the way through the deceleration. Reverse flow is now present at the inner bend at all stations,

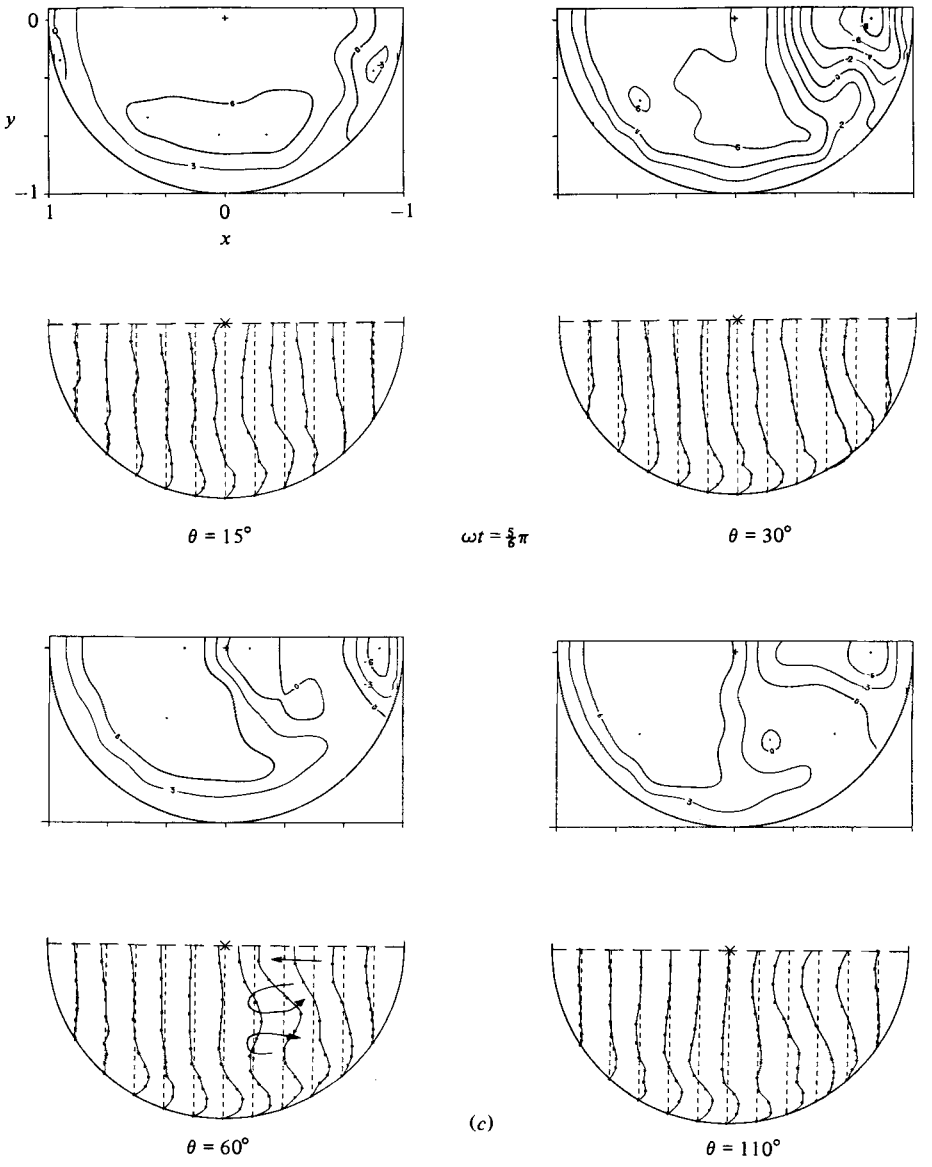

(c)

FIGURE 7(c). For caption see p. 19.

and probably extends all the way to the inlet of the pipe. The area of the cross-section occupied by the reversed flow has expanded outward from the inside bend, though not appreciably downward along the pipe wall. At $\theta = 110°$ the area where the imbedded helical motions are located also exhibits negative axial velocities. These appear to be associated with the bulk deceleration of the fluid, rather than the inside-bend reverse flow. The negative-axial-velocity region near the centre of the pipe at $\theta = 60°$ may be the result of upward convection of inner-bend reversed-flow fluid which was previously in the region of the secondary maximum. Upward convection of the fluid in the region of the secondary maximum 'ridge' is also evident at $\theta = 30°$.

Separation and reattachment of the axial flow at the outside bend appears to have occurred in the vicinity of $\theta = 15°$, though not farther downstream. Apparently the

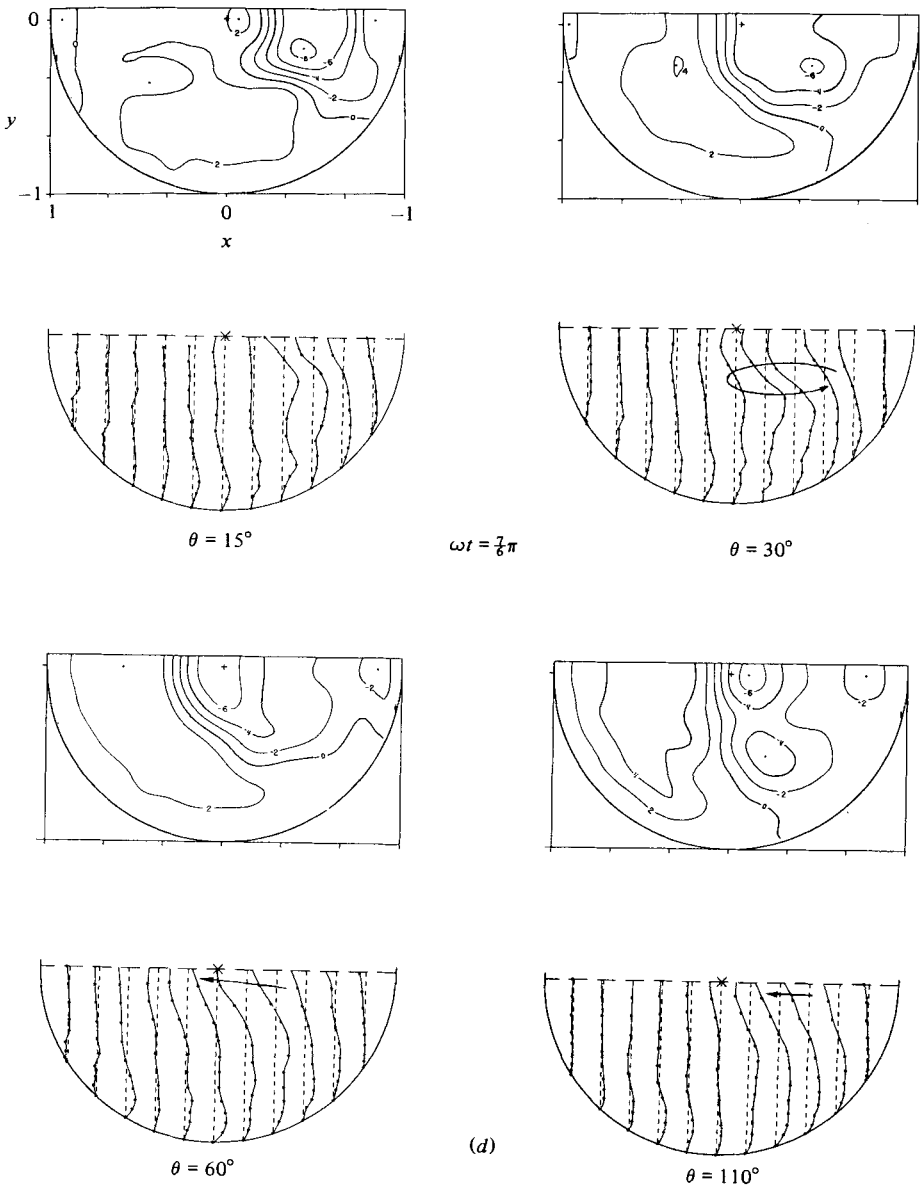

FIGURE 7(*d*). For caption see p. 19.

adverse pressure gradient is sufficient to cause separation of the outside-bend boundary layer here, before it gains additional momentum downstream due to the outward shift of the maximum axial velocity.

Figure 7(*d*) shows the situation at time instant $\omega t = \frac{7}{6}\pi$, which is just following the time when the flow rate passes through its minimum. There is now reverse axial flow throughout the inner bend of the pipe, at all streamwise locations. The area of reverse flow increases with θ, and at $\theta = 110°$ occupies about half of the cross-section.

The secondary motion exhibits some interesting features. It is present mainly in the inner-bend region and consists of a strong outward jet-like motion concentrated near the midplane, accompanied by a more distributed inner motion below. As

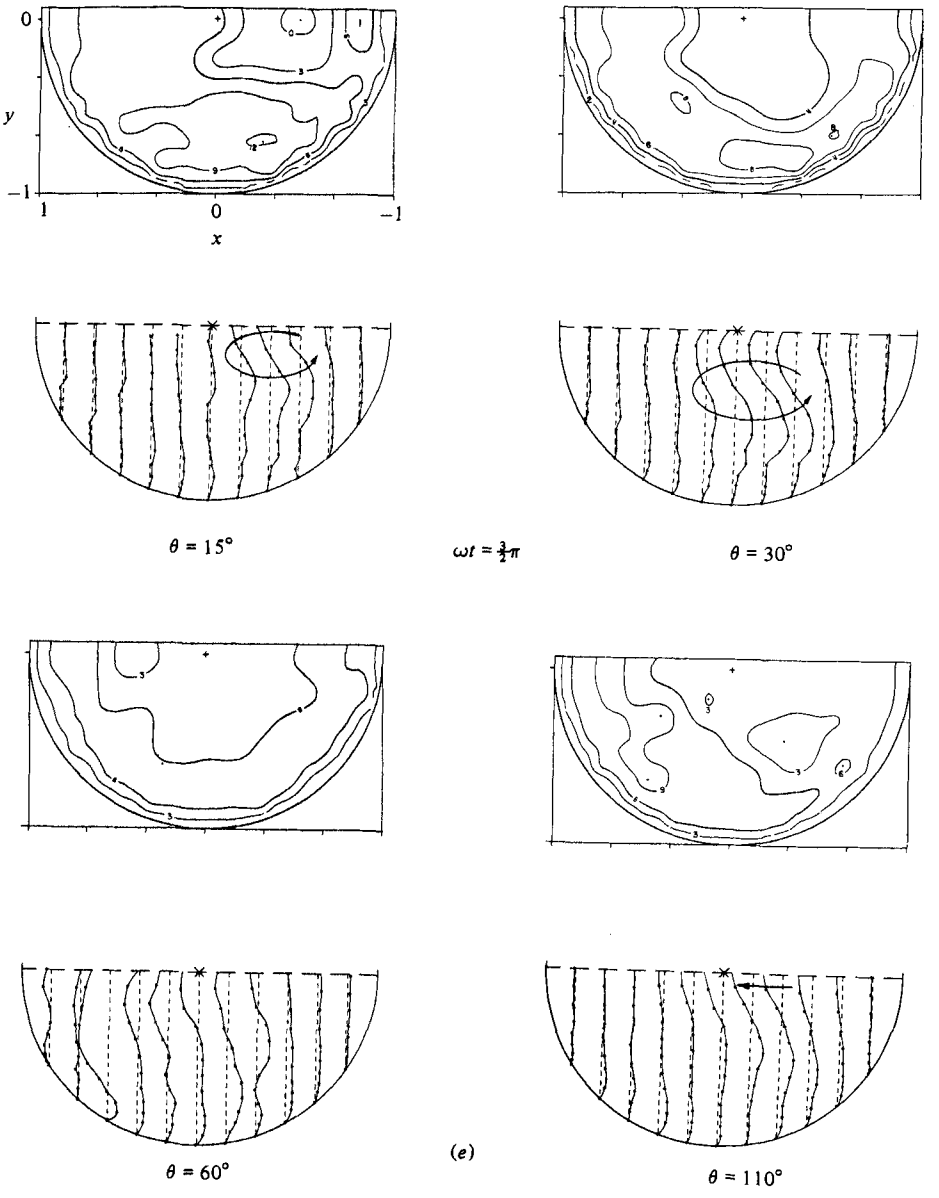

FIGURE 7(e). For caption see facing page.

suggested in the data for the 30° station, there is indication of an imbedded helical motion in the inner bend region.

At time instant $\omega t = \frac{3}{2}\pi$, shown in figure 7(e), the flow is well into its accelerative phase. Negative axial velocities have disappeared, and at stations $\theta = 30°$ and 60° a ridge has formed in the isotachs separating the fluid near the centre of the pipe from that near the wall. The secondary motion at $\theta = 15°$ and 30° are helix-like, while those at 60° and 110° are more jet-like. The strong secondary motions near the outer bend at $\theta = 60°$ is probably the result of the secondary 'jet' reaching the boundary layer at the outside bend. It may be noted that, for $x \lesssim -0{\cdot}5$, the secondary motion consists only of inward-moving fluid.

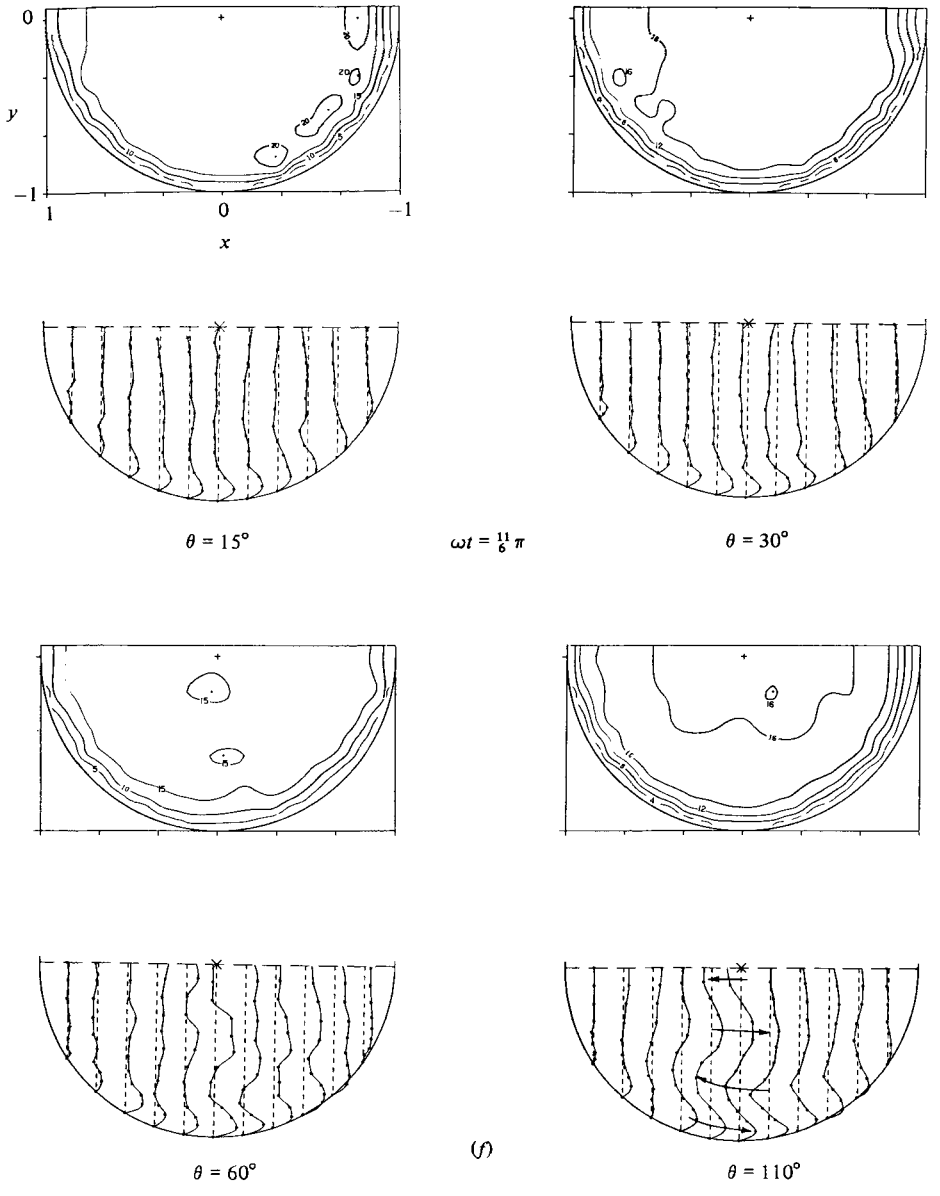

FIGURE 7. W-velocity isotachs and U-velocity profiles at different π-locations at various instants of time in the cycle for experiment 2: (*a*)–(*f*): $\omega t = \frac{1}{6}(2n+1)\pi$, $n = 0$–5.

The final stages of flow acceleration are shown in figure 7 (*f*), corresponding to time instant $\omega t = \frac{11}{6}\pi$. At $\theta = 7°$ the secondary motion is confined mainly to the inwardly moving circumferential boundary layer, and there is relatively little motion in the core of the flow. At $\theta = 30°$ the strength of the outward motion in the core has increased in the core region for $x \lesssim 0{\cdot}2$, but remains fairly uniform. However, at $\theta = 60°$ and 110° one finds four distinct regions of secondary motion, two outward and two inward. We believe that this complicated motion is associated with 'ridges' in axial velocity remarked on earlier. Referring to the isotachs at $\theta = 60°$, one

observes that the two islands of high axial velocity correspond in location with the outward-moving regions of secondary flow. Evidently the same imbalance between lateral acceleration ($\approx W_0^2/L$) and pressure gradient $(1/\rho)\,\partial p/\partial \hat{x}$ which gives rise to the overall Dean circulation also causes the local helical circulations. Of course, these local circulations themselves influence the distribution of axial velocity, so the overall interaction is complex and difficult to describe quantitatively.

Although it may be tempting to relate these local circulations to the recently discovered bifurcation of the fully developed two-vortex Dean circulation into a four-vortex solution (Dennis & Ng 1982; Nandakumar & Masliyah 1982) it seems clear that the two phenomena are distinctly different. In the fully-developed-flow case, the second pair of vortices appears at the outer bend, whereas the imbedded helical motions are located in a region closer to the inner bend. Moreover, for steady flow, as described in I, these motions appear only in the flow-development region, and disappear as the fully developed flow is approached.

We may summarize the sequence of events that take place during a flow cycle as follows. Beginning at $\omega t = \frac{1}{6}\pi$, just after peak flow rate, the fluid at the inside bend in the downstream sections of the pipe first begins to decelerate. This deceleration is accompanied by the appearance of a jet-like outward secondary motion. Further deceleration of the inner bend fluid causes the secondary jet to strengthen, which then leads to the formation of the imbedded helical motions, which may, in a kinematical sense, be likened to a 'mushrooming' behaviour of the secondary jet. Part of the core flow is trapped between the wall viscous layer and the edge of the secondary-jet region, which leads to the formation of the axial-velocity ridge.

As deceleration proceeds, negative axial velocities appear, first in the downstream portions of the pipe, giving rise to a global-type separated flow in this part of the pipe. This separation propagates upstream until, near the end of the decelerative phase of the cycle, the inner-bend regions are completely occupied with reverse axial flow and strong outward secondary flow.

Axial flow acceleration, following the minimum in the flow rate, first occurs in the inner-bend fluid at the pipe entrance. This acceleration causes the downstream inner-bend fluid, which is still undergoing reverse flow, to detach from the inner bend and move outward, allowing downstream-moving core fluid to flow in and around the reverse-flow region. Further into the accelerative portion of the cycle, the inwardly moving core fluid from the upper and lower halves of the section collides at the inner bend, and high axial velocities appear in this region. Near the end of the cycle, the axial velocities at the inner bend begin to decrease at the downstream sections, and the secondary jet is formed.

6. Comparison with other experiments

The experimental investigations most relevant to the present one are the two studies of Chandran, Yearwood & Weiting (1979) and Chandran & Yearwood (1981). Both of these studies were concerned with the simulation of entry flow into the aorta, and utilized pulsatile waveforms chosen to model aortic flow (a systolic interval followed by a diastolic interval) rather than the sinusoidal waveform employed in the present work. However, the parameters associated with these studies are not much different from those of our second experiment; Chandran *et al.* used a pipe with $\delta = \frac{1}{10}$, and the alternative Dean number and Womersley parameter values were $\kappa = 320$ and $\alpha_w = 20{\cdot}8$.

In the first of the two studies flow-visualization observations were made and axial

velocities were obtained by means of a single-component hot-film probe. In the second study the velocity data were obtained using a three-component hot-film probe, which was traversed across the horizontal ($y = 0$) and vertical ($x = 0$) planes of symmetry at several streamwise locations. Their general conclusions are consistent with ours. They observed a strong reversed flow along the inner wall of the tube during diastole (aortic valve closed), which increased with θ in strength and in the extent of the cross-section it occupied. They also observed shifts in the location of the maximum value of W (along the plane $y = 0$) with θ during systole, with the maximum occurring near the outer wall for $\theta \approx 20°$, moving toward the inner wall for $\theta \approx 60°$, and returning to the outer wall for $\theta \approx 100°$. Their variations and excursions in $W_{\max}(y = 0)$ are somewhat greater than, though not in conflict with, what we observed.

Comparisons with the secondary velocity data of Chandran *et al.* are more difficult to make, since they obtained data only along $y = 0$ and $x = 0$. Further, there was an observed lack of symmetry about the plane $y = 0$, which was attributed to disturbances introduced by the prosthetic valve used to simulate the aortic valve. However, they conclude that 'trapped vortical motions are seen to occur at the inner walls of the tube at plane E [$\theta \approx 100°$], having originated as rotational motions in the boundary layer as a result of circumferential flows toward the inner wall in the regions of plane B [$\theta \approx 49°$] and C [$\theta \approx 60°$], where the initial shift in axial momentum is first observed.' Our secondary-velocity data, together with those presented in I, suggests a slightly different explanation for the occurrence of trapped helical motions. In the steady-flow experiments for I, for $\delta = \frac{1}{7}$ and $\kappa = 183$, where secondary maxima (i.e. ridges) in the axial velocity profiles were not observed, there was likewise no appearance of trapped helical motions, whereas for $\delta = \frac{1}{7}$ and $\kappa = 372$, where secondary maxima in W were observed, trapped helical motions were also present. The joint occurrence of the secondary maxima and the trapped helical motions is also evident in the present data. As mentioned earlier, the phenomenon involved is believed to be a result of local imbalances between centrifugal force and pressure gradient in the developing region of the flow, of the same nature as that responsible for the global Dean circulation in fully developed flow. Since these imbedded helical motions are observed under both steady and unsteady flow conditions, pulsatility is not the determining factor in their appearance. Whether they are present or not seems to depend primarily on κ; for $\kappa = 183$ they were absent, while they were present for $\kappa = 372$ in our experiments and for $\kappa = 320$ in those of Chandran *et al.* (1979). More data are required to fix the value of κ at which they first appear.

7. Comparisons with theory

Given the complicated nature of this unsteady three-dimensional flow, it is not surprising that no theorectical results, either analytical or numerical, have yet been obtained that adequately describe it. Nevertheless, the studies that have been attempted expose some interesting fluid-dynamical phenomena which may be present in the flows under consideration and it is therefore of some value to examine the predictions of these studies.

The problem of purely oscillatory flow (no mean component) in a curved tube has been studied by Lyne (1971), Zalosh & Nelson (1973) and Chandran, Swanson & Ghista (1974). The most interesting prediction of these studies is that for values of α_w greater than a certain critical value the secondary flow within the central regions of the cross-section reverses sign, and is directed from the outside bend toward the

inside one. The explanation for this phenomenon is that the Dean circulation is confined to narrow Stokes layers adjacent to the upper and lower walls, and the outward-returning fluid at the outer edges of these layers drags with it adjacent fluid within the core, thus setting up an additional circulation within the core of opposite sign to the Dean circulation. This conclusion has been confirmed experimentally by Lyne and by Munson (1975).

For small values of secondary Reynolds number $R_s = \delta W_{AC}^2/\omega\nu$, where $W_{AC} = Q_{AC}/\pi a^2$, Zalosh & Nelson found that the transitions from outward to inward secondary motion within the central region of the core occurred at a value $\alpha_w \approx 9$. Munson's data suggest a slightly higher value, about 12. The crossover value of α_w appears to be only weakly dependent on R_s.

It is of interest to see whether we can draw any conclusions from the present data regarding the occurrence of 'inward centrifuging' in the presence of a non-zero steady component of axial velocity. The most appropriate location at which comparisons might be made is at the farthermost-downstream station, where the flow is closest to being fully developed. For experiment 1 with $R_s \approx 6{\cdot}4$ and $\alpha_w = 8$, at $\theta = 135°$ the value of $U(0,0)/W_{AC}$ is typically of the order of $\frac{2}{3}$, while for experiment 2, with $R_s \approx 231$ and $\alpha_w = 12{\cdot}5$, at $\theta = 110°$, $U(0,0)/W_{AC}$ is of the order of $\frac{1}{5}$. There is apparently a trend toward decreasing $U(0,0)/W_{AC}$ with increasing α_w although, if a reversal does occur, it is at a higher value of α_w than is found in the case of pure oscillatory flow.

Smith (1975) has examined the character of the various fluid motions that occur in fully developed pulsatile flow in a curved pipe when a steady-flow component is also present. He identifies ten separate regimes depending on the values assumed by three parameters, the Dean number D, the secondary Reynolds number R_s and the frequency parameter $\beta = \sqrt{2}/\alpha_w$. The Dean number is defined as $D = Ga^3\delta^{\frac{1}{2}}/\rho\nu^2$, where G is the pressure gradient associated with the steady-flow component of the motion; note that D is smaller by the factor $\sqrt{2}$ than the Dean number employed by Collins & Dennis (1975) and by Dennis (1980). For certain limiting values of the triad (D, R_s, β) solutions are obtained, while for others only the forms of the solutions are sketched.

To make comparisons with Smith's work, the values of D corresponding to our two experiments must be established. This cannot be done directly, since G is unknown. However, Collins & Dennis have given the values of κ corresponding to the values of D for the cases they have calculated, and these correspondences can be used to establish approximate values of D for the two experiments.† In this way (and accounting for the factor $\sqrt{2}$) it is found that $D \approx 750$ for the first experiment, and $D \approx 3540$ for the second. In terms of the parameters employed by Smith, we then have

$$D = 750, \quad R_s = 6{\cdot}4, \quad \beta = 0{\cdot}177 \quad \text{for experiment 1;}$$

$$D = 3540, \quad R_s = 230, \quad \beta = 0{\cdot}113 \quad \text{for experiment 2.}$$

Referring to Smith's classifications we find that experiment 1 most closely corresponds to his case V ($D \gg 1$, $\beta \sim D^{-\frac{1}{3}}$, $R_s \sim 1$), while experiment 2 most closely corresponds to his case X ($D \gg 1$, $\beta \sim D^{-\frac{1}{3}}$, $R_s \sim D^{\frac{2}{3}}$).

For case V Smith concludes that the motion is largely a steady one. The oscillatory part of the pressure gradient merely contributes to amplitude variations in the basic steady flow. This is exactly what was found in experiment 1.

† In fact, for a developing flow $G = G(\hat{z})$, so that, although κ is a constant, D is not. The correspondence between D and κ is thus only strictly valid in the downstream fully developed limit.

The situation pertaining to Smith's case X is more complicated. With $\beta = \tilde{l}D^{-\frac{1}{2}}$, Smith finds that the forms of the solutions can be discussed only in the two limits $\tilde{l} \ll 1$ and $\tilde{l} \gg 1$, a full numerical treatment being needed for the general case. Unfortunately, as we can easily see from the values listed above for experiment 2, $\tilde{l} \approx 1{\cdot}72$, so this experiment does represent the general case. This case, according to Smith, is characterized by coincidence of the Stokes layers and the steady and secondary viscous layers. The secondary motions can be pulsatile, and the steady and unsteady axial pressure gradients couple together to affect the axial velocity, while the unsteady secondary motions are driven mainly by the steady pressure gradient. The secondary motions may be reversible (in the sense of Lyne's findings) but are definitely outward for small $\tilde{l}$.

It is difficult to determine to what extent Smith's description of the flow characteristics of case X is relevant to the data of the second experiment, since Smith's analysis pertains to a fully developed flow, while it is highly likely that even at the farthermost-downstream stations $\theta = 110°$ the flow in experiment 2 is not yet fully developed.† One can conclude that, at least qualitatively, Smith's description is not at variance with what is observed, and that the features that distinguish the properties of the flows of the first and second experiments might be appropriately classified by the ranges of values assigned to the basic parameters D, R_s and β. This might prove to be an important guide to future analysis.

The final theoretical result we shall discuss is the analysis of Singh, Sinha & Aggarwal (1978). In principle, this analysis is more applicable to the present results than those previously discussed, since it deals directly with pulsatile entry flow within a curved circular pipe. It is in fact an extension of the steady-entry-flow analysis of Singh (1974). Singh *et al.* consider two pulsatile waveforms, one a sinusoidal oscillation superimposed on a steady flow, given by

$$Q = 1 + \frac{Q_{AC}}{Q_{DC}} \sin \tau$$

and one of a more physiological character. Only the results for the sinusoidal waveform will be considered here.

The approach of Singh *et al.* is essentially to divide the flow field into a boundary-layer region and an inviscid core, obtain appropriate expansions of the flow equations in each region, and then match the expansions to like order. For example, the axial boundary-layer flow is a Blasius flow perturbed by contributions due to wall curvature, unsteadiness and the displacement effect. The results are valid within the limitations (*a*) $\hat{z}/(aL)^{\frac{1}{2}} \lesssim 1$, and (*b*) $\hat{z}\omega|dQ/d\tau|/W_0 Q^2 \lesssim 0{\cdot}5$. Limitation (*b*) disqualifies experiment 2 over much of its cycle, while limitation (*a*) restricts the region of application of the analysis for experiment 1 to $\theta \lesssim 13°$. Hence only the first streamwise station of experiment 1, $\theta = 7°$, can be properly compared with this analysis.

The calculation of the distribution of the axial wall shear stress τ_{wz} around the circumference of the pipe at $\theta = 7°$ according to equation (36) of Singh *et al.* (1978) yields only a very modest variation of τ_{wz} with α, and this is consistent with the shapes of the isotachs (apart from the local separations at $\alpha = 0$ and π) at this station. For the azimuthal (α-direction) secondary-velocity boundary layer the authors find

$$\frac{v_\alpha}{W_0} = Q\delta z \sin \alpha \, g'(\zeta),$$

† Austin (1971) gives for the flow-development length $\theta_d = 49(\kappa\delta)^{\frac{1}{2}}$ (deg) for a curved pipe with a parabolic entry flow profile. Although the data of I suggest that this may underestimate the entry length required for a uniform entry flow profile, if we use this criterion we find $\theta_d = 184°$:

where $\zeta = (1-\hat{r}/a)\ (aW_0\ Q/2z\nu)^{\frac{1}{2}}$ and $g'(\zeta)$ is a function whose form can be deduced from figure 8(*b*) of Singh (1974). Thus v_α is predicted to be quasisteady, grow linearly in amplitude with z and vary sinusoidally with α. The thickness of the v-boundary layer is predicted to vary as $z^{\frac{1}{2}}$, and, at a given z, thicken and thin inversely as $Q^{\frac{1}{2}}$. The secondary-velocity data at $\theta = 7°$ do have a quasisteady character, and the variation of $(v_\alpha)_{\max}$ is roughly sinusoidal except in the vicinity of $\alpha = 0$ due to the local separation there. However, the thickness of the layer appears to be sensibly constant in time and not dependent on Q. Also, the predicted thickness of the secondary-velocity boundary layer, as estimated from the value of ζ at which Singh's secondary velocities asymptote to zero, is greater than what is observed experimentally.

While the analysis of Singh *et al.* may provide a useful set of starting conditions for a numerical analysis of pulsatile entry flow into a curved pipe, it seems evident that, just as in the case of steady entry flow, a boundary-layer-type analysis is inadequate for a full solution of the problem. Indeed, the many scalings required by Smith to describe the fully developed case indicate that a Blasius scaling with perturbations due to pulsatility and curvature is doomed to failure. Even in the case of steady entry flow, the numerical calculations of Stewartson, Cebeci & Chang (1980) reveal a singular behaviour of the axial wall shear at $\hat{z}/(aL)^{\frac{1}{2}} \approx 0{\cdot}94$ at $\alpha = \pi$, which is missed out completely by a conventional boundary-layer analysis. Stewartson's predictions for $\hat{z}$ less than this critical value have been confirmed experimentally by Talbot & Wong (1982).

8. Concluding remarks

The measurements reported here reveal several features of particular interest. We observe that the general characteristics of unsteady curved-pipe entry flow appear to be classifiable in terms of the same three parameters as are used to classify fully developed pulsatile flows: the Dean number (or the alternative Dean number), the secondary Reynolds number and the frequency parameter. Whether the flow is quasisteady, as was found in experiment 1, or involves complex interactions between the axial and secondary velocities, as was found in experiment 2, may depend on both R_s and κ in the case of fully developed flow, but mainly on κ for entry flow since these complex interactions are observed in steady entry flow as well. Among the complex interactions are helical motions imbedded within the Dean circulation which appear to be associated with ridges in the axial velocity profiles, as in the case of steady flow.

The results of experiment 2 indicate that reversal of the bulk flow as a whole is not required for the occurrence of separation and reversed flow over part of the cycle. When separation and reversed flow do occur, the separation first appears in the downstream inner-bend region of the pipe (which is to be expected since this is the region of least axial momentum of the core fluid), and propagates upstream as the decelerative phase of the cycle progresses.

The occurrence or non-occurrence of flow reversal must depend in some fashion on the relative magnitudes of the parameters R_s, κ and α_w, although the data presented here are not sufficient to establish this dependency. From a physical point of view, a possible indicator of flow reversal would be the ratio of the pressure gradients associated with the steady and unsteady axial velocity components. In the theory for fully developed flow this ratio is given by

$$P_r = \frac{G}{\rho\omega W_{AC}} = \frac{D}{\alpha_w^3 R_s^{\frac{1}{2}}} = \frac{D\beta^3}{(8R_s)^{\frac{1}{2}}}.$$

Smith's case V corresponds to $P_r \sim 1$, while case X corresponds to $P_r \ll 1$. Assuming that this pressure ratio will not be much different for developing flow, and that the theoretical Dean number D can be approximately related to the experimental alternative Dean number κ through the work of Collins & Dennis, we find $P_r = 0{\cdot}58$ for experiment 1 and $P_r = 0{\cdot}12$ for experiment 2. Although the two values are not dramatically different, they may be suggestive of the ranges of values of P_r that are associated with reversing and non-reversing flows.

This work was supported by the National Science Foundation under Grant no. MEA 8116360. The authors are indebted to Dr David J. Peake for helpful discussions.

REFERENCES

ADLER, M. 1934 *Z. angew. Math. Mech.* **14**, 257.

AGRAWAL, Y. C., TALBOT, L. & GONG, K. 1978 *J. Fluid Mech.* **85**, 497.

AUSTIN, L. 1971 The development of viscous flow within helical coils. Ph.D. thesis, University of Utah.

CHANDRAN, K. B., SWANSON, W. M. & GHISTA, D. M. 1974 *Ann. Biomed. Engng* **2**, 392.

CHANDRAN, K. B. & YEARWOOD, T. L. 1981 *J. Fluid Mech.* **111**, 59.

CHANDRAN, K. B., YEARWOOD, T. L. & WEITING, D. W. 1979 *J. Biomed.* **12**, 793.

CHOI, U. S., TALBOT, L. & CORNET, I. 1979 *J. Fluid Mech.* **93**, 465.

COLLINS, W. M. & DENNIS, S. C. R. 1975 *Q. J. Mech. Appl. Math.* **28**, 133.

DENNIS, S. C. R. 1980 *J. Fluid Mech.* **99**, 449.

DENNIS, S. C. R. & NG, M. C. 1982 *Q. J. Mech. Appl. Math.* **35**, 305.

GONG, K. O. 1979 Experimental study of unsteady entrance flow in a curved pipe. *Univ. of Calif. Coll. Engng, Berkeley, Rep.* FM-79-1.

LYNE, W. H. 1971 *J. Fluid Mech.* **45**, 13.

MUNSON, B. R. 1975 *Phys. Fluids* **18**, 1607.

NANDAKUMAR, K. & MASLIYAH, J. H. 1982 *J. Fluid Mech.* **119**, 475.

NEREM, R. M. & CORNHILL, J. F. 1980 *Trans. A.S.M.E.* K: *J. Biomech. Engng* **102**, 181.

SINGH, M. P. 1974 *J. Fluid Mech.* **65**, 517.

SINGH, M. P., SINHA, P. C. & AGGARWAL, M. 1978 *J. Fluid Mech.* **87**, 97.

SMITH, F. T. 1975 *J. Fluid Mech.* **71**, 15.

STEWARTSON, K., CEBECI, T. & CHANG, K. C. 1980 *Q. J. Mech. Appl. Math.* **33**, 59.

TALBOT, L. & WONG, S. J. 1982 *J. Fluid Mech.* **122**, 505.

TOBAK, M. & PEAKE, D. J. 1982 *Ann. Rev. Fluid Mech.* **14**, 61.

ZALOSH, R. & NELSON, W. G. 1973 *J. Fluid Mech.* **59**, 693.